Malaysian Journal of Analytical Sciences (MJAS)



Published by Malaysian Analytical Sciences Society

RECOVERY OF PHOSPHATE FROM ARTIFICIAL HUMAN URINE USING MAGNESIUM-MODIFIED BIOCHAR FOR IMMOBILIZATION OF LEAD IN SOIL

(Pemulihan Fosfat daripada Urin Manusia Tiruan Menggunakan Biochar yang diubah suai Magnesium Untuk Imobilisasi Plumbum dalam Tanah)

Soon Kong Yong ^{1*} Nurul Fariha Mohd Idrus¹, Nur Qursyna Boll Kassim², Azwan Mat Lazim³, and Robert Thomas Bachmann⁴

¹Soil Assessment and Remediation Research Group,
Faculty of Applied Sciences,
Universiti Teknologi MARA, 40450 Shah Alam, Selangor, Malaysia
²Soil Conservation and Management Research Group,
Faculty of Plantation and Agrotechnology,
Universiti Teknologi MARA, 40450 Shah Alam, Selangor, Malaysia
³Faculty of Science and Technology,
Universiti Kebangsaan Malaysia, 43600 Bangi, Selangor, Malaysia
⁴Green Chemistry & Sustainable Engineering Technology Cluster,
Section of Environmental and Polymer Engineering Technology,
Malaysian Institute of Chemical and Bioengineering Technology,
Universiti Kuala Lumpur, 78000 Alor Gajah, Malacca, Malaysia

*Corresponding author: yongsk@uitm.edu.my

Received: 22 September 2022; Accepted: 27 February 2023; Published: 19 April 2023

Abstract

Magnesium-modified biochar (MB) is used to recover phosphate (PO₄³⁻) from urine by struvite precipitation. Pyrolysis of sawdust (SD) at 700°C and subsequent impregnation with MgO₂ produced MB. Virgin and spent MB were characterized for proximate analysis, surface morphology, elemental composition, specific surface area, and functional groups using thermogravimetric analysis (TGA), scanning electron micrography (SEM), energy dispersive X-ray (EDX) analysis, surface area analysis, and Fourier transform infrared (FTIR) spectroscopy, respectively. The batch sorption experiments were conducted on MB using artificial human urine (AHU), where residual PO₄³⁻ was quantified by colorimetry. Sorption data were analyzed using various isotherm (i.e., Langmuir and Freundlich) and kinetic models (i.e., pseudo-first and pseudo-second-order) for elucidation of sorptive potential and mechanism. Pyrolysis of SD produced porous sawdust biochar (SB) with a high surface area. However, modification with MgO₂ decreased the surface area of MB, possibly due to the loss of micropores from oxidation and deposition of struvite as confirmed by SEM-EDX analysis. FTIR analysis showed that polar functional groups such as carboxylate (1641 cm⁻¹), phenolate (1300 cm⁻¹), and amide (1674 cm⁻¹) were mainly involved in the Mg²⁺ and PO₄³⁻ adsorption. The PO₄³⁻ sorption capacity for MB was 8967 mg/g at a sorbent/solution ratio of 0.1 g/L after 120 min of contact time. Sorption of PO₄³⁻ occurred on a heterogeneous MB surface with a possible multilayer adsorption mechanism. The kinetic study suggested that the sorption of PO₄³⁻ by MB was a chemisorption process. The presence of Mg in MB aided the formation of struvite in MB and enhanced the recovery of PO₄³⁻ from

AHU. Spent MB exhibited higher ability in immobilizing soil Pb compared to ground magnesium limestone (GML) at a similar application rate (5% w/w). Spend MB can be recovered as fertilizer or immobilizing heavy metals such as lead in soil.

Keywords: oxidized biochar, magnesium peroxide, struvite, phosphate recovery, human urine

Abstrak

Biochar yang diubah suai dengan magnesium (MB) digunakan untuk memulihkan fosfat (PO43-) daripada air kencing melalui pemendakan struvite. Pirolisis habuk papan (SD) pada 700°C dan impregnasi seterusnya dengan MgO2 menghasilkan MB. Keduadua MB mentah dan terpakai dicirikan pada analisis proksimat, morfologi permukaan, komposisi unsur, luas permukaan spesifik dan kumpulan berfungsi telah dijalankan menggunakan penganalisis termogravimetrik (TGA), pengimbasan mikrografi elektron (SEM), analisis sinar-X penyebaran tenaga (EDX), penganalisis luas permukaan, dan spektroskopi Inframerah transformasi Fourier (FTIR), masing-masing. Eksperimen jerapan telah dijalankan pada MB menggunakan air kencing manusia tiruan (AHU), di mana sisa PO₄3- ditentukan dengan teknik kolorimetri. Data jerapan dianalisis menggunakan pelbagai model isoterma (iaitu, Langmuir and Freundlich) dan kinetik (iaitu, pseudo-tertib-pertama and pseudo-tertib-kedua) untuk penjelasan potensi dan mekanisme jerapan. Pirolisis SD menghasilkan biochar (SB) berliang dengan luas permukaan yang tinggi. Walau bagaimanapun, pengubahsuaian dengan MgO2 mengurangkan luas permukaan MB, mungkin disebabkan oleh kehilangan mikropori daripada pengoksidaan dan pemendapan struvite seperti yang disahkan oleh analisis SEM-EDX. Analisis FTIR menunjukkan kehadiran kumpulan berfungsi polar seperti karboksilat (1641 cm⁻¹), fenolat (1300 cm⁻¹), dan amida (1674 cm⁻¹) terlibat terutamanya dalam penjerapan Mg²⁺ dan PO₄³⁻. Kapasiti penyerapan PO₄³⁻ untuk MB ialah 8967 mg/g pada nisbah sorben/larutan 0.1g/L selepas 120 minit masa sentuhan. Penyerapan PO₄³⁻ berkemungkinan berlaku pada permukaan MB heterogen dengan mekanisme penjerapan berbilang lapisan. Kajian kinetik menunjukan bahawa proses penjerapan PO43- oleh MB adalah melalui proses kimia. Kehadiran Mg dalam MB membantu pemendakan struvite dalam MB, dan meningkatkan prestasi pemulihan PO43- daripada AHU. MB terpakai lebih cekap dalam imobilisasi plumbum di dalam tanah berbanding dengan batu kapur magnesium terkisar (GML) pada kadar penggunaan yang sama (5 % w/w). MB terpakai boleh dikitar semula sebagai baja atau merawat tanah yang tercemar dengan logam berat seperti plumbum.

Kata kunci: biochar teroksida, magnesium peroksida, struvite, pengambilan semula fosfat, urin manusia

Introduction

Phosphorus is a macronutrient that occurs naturally in the orthophosphate (PO₄³-) form and is essential for all living organisms [1]. According to the Malaysian Department of Environment, the permissible level of PO₄³⁻ in effluent discharge is 5 mg/L [2]. Excessive PO₄³- in aquatic environments may eutrophication. Human urine is managed through a modern sewer system and treated biologically to effectively remove PO₄³⁻ [3]. Despite the abundance of PO₄³⁻ in human urine, its recovery is associated with the risk of pathogen infection and adverse effects of residual pharmaceutical products. Despite the challenges, human urine is a renewable source of PO₄³⁻ that can be recovered for crop production [4]. Adsorption is an energy-efficient and low-cost technique for recovering PO₄³⁻ from human urine [5]. Furthermore, the yield of PO₄³- recovery can be improved by slightly increasing the pH value of human urine [6].

Biochar is a sorbent commonly used for the removal of

pollutants from the environment. Pyrolysis of agricultural biomass at a high temperature (i.e., >500 °C) and anoxic conditions can produce carbon-rich and porous biochars [7]. The surface of low-temperature biochars often contains plenty of polar functional groups (i.e., phenol and hydroxyl [8]. A slightly alkaline condition allows deprotonation of the polar functional groups and may be used for adsorbing pollutants that possess a net positive charge [9]. Moreover, biochar is considered a recalcitrant organic carbon that can withstand microbial decomposition. The application of biochar allows the storage of carbon in the soil, reduces greenhouse gas emissions, and helps combat climate change [10]. The improvement of soil fertility by the addition of biochar helps the greening and reclamation of the polluted land and increases the capacity for holding cationic nutrients [11].

Residual minerals in biochar consist mainly of oxides of alkaline (i.e., K₂O) or earth alkaline metals (i.e., CaO, MgO), providing an alkaline condition that can improve

electrostatic attraction and precipitation of PO₄³⁻ ions [12]. Moreover, polar functional groups may react with Ca2+ or Mg2+ cations to acquire a positively charged surface and become a medium for binding PO₄³⁻ ion [13]. However, the CaO content in biochars may be insufficient for effectively recovering PO₄³⁻ from human urine. Various methods have been used for artificially introducing Ca and Mg into biochar. Magnesium chloride (MgCl₂) and oxide (MgO) were commonly used for modifying biochar [14]. An activation of biochar with MgO has successfully increased the surface functional group, porosity, surface area, and PO₄³removal [15]. The introduction of Mg is often associated with a high PO₄3- removal due to the precipitation of struvite, which is formed with the addition of phosphate into a portion of ammonium and magnesium at equal ratio concentrations [16].

Even though the pyrolysis process at high temperature produces porous biochar, possible decarboxylation may cause a net loss of polar functional groups such as carboxylate and phenolate groups [17]. The presence of the negative-charged polar organic functional groups on the biochar surfaces is crucial for its function in soil fertility, including the retention of essential cations such as Mg²⁺ [18]. Oxidation can be introduced to improve the negative surface of high-temperature biochars. Recent studies have shown the great potential of combining electro-oxidation for improving the porosity and capacity of biochar to retain Mg for recovering PO₄³- [19]. Alternatively, biochar can be chemically oxidized and impregnated with Mg simultaneously using magnesium peroxide (MgO₂). The oxidation and subsequent Mg-deposition can be controlled by decreasing and increasing the solution pH, respectively. The slow dissolution of MgO₂ in slightly acidic water at room temperature allows the slow release of dissolved oxygen for minimizing damage to the microporous structure of the biochar during oxidation. Upon complete dissolution of MgO2, the adsorption and precipitation of soluble Mg2+ can be enhanced by slowly increasing the solution pH. In this study, sawdust is a widely available solid waste from the sawmill and was used as the precursor for the production of biochar.

Materials and Methods Preparation of sawdust (SD) and sawdust biochar (SB)

About 10 kg of SD was collected from a furniture processing plant at Klang, Selangor. The SD was washed with tap water and oven-dried overnight at 105 °C. Then, the SD was pulverized using a mixer grinder and sieved to a particle diameter of <150 μ m. About 500 g of the SD was converted into SB through slow pyrolysis at 700 °C in a furnace with nitrogen gas at a flow rate of 10 L/min. The pH value of the resulting SB was measured with a pH meter at SB/DI water mass ratio of 1:10 [20]. The SB was washed further with warm DI water until it reached a pH value of 8. The SB was then placed in the lid-covered metal crucibles and allowed to dry in a dehydrating cabinet at 60 °C for 24 h.

Modification of SB with MgO₂

The preparation of MgO₂-modified biochar (MB) followed the method described by Tan et al. [21] and is optimized at 5% w/v MgO2 concentrations. Thirty millilitres of each MgO₂ solution were mixed with 1.0 g SB. The solution was adjusted to a pH value of 2 by adding 65% HNO₃ drop by drop using an auto titrator. The mixture was agitated for a few minutes until the effervescence ceased, and then agitated for a further 30 min. The mixture was allowed to rest overnight at room temperature (25°C). The pH of the biochar was adjusted to a pH value between 6.0 and 6.5 by adding 1.0 M NaOH using an auto titrator and then agitated for 4 h with a magnetic stirrer at room temperature. Then, MB was collected after filtration, oven-dried at 90 °C, and then pulverized to a desired particle size of 0.20-0.45 mm [21].

Chemical characterization for SD, SB, and MB

Surface morphology and elemental composition were investigated using scanning electron microscopy (SEM) with energy dispersive X-ray spectroscopy (EDX) (Hitachi TM3030plus). About 1 mg of sample was coated with a thin layer of carbon and mounted on a copper stub using double-stick carbon tape. Thermal degradation analysis was conducted on the as-receive SD (10 mg) using a thermogravimetric analyzer (TGA) (Setaram Setsys Evolution TGA-DTG/DSC High Temperature (2400) instrument at a heating rate of

10°C/min, and a peak temperature of 900 °C in a nitrogen atmosphere. The **TGA** and differential thermogravimetric (DTG) data were analyzed using AKTS Thermokinetics software. Major inorganic elements were determined using the Association of Official Analytical Chemists (AOAC) method of acid digesting the samples (1.0 g) for multi-elemental analysis by ICP-OES. The presence of functional groups on samples was studied using Fourier transform infrared (FTIR) spectroscopy. About 5 mg of sample was mixed with potassium bromide KBr at approximately 0.1% w/w and pressed into pellets. The spectra of the samples were collected using an FTIR spectrometer (Perkin Elmer) by averaging 32 scans in the range of 400 to 4000 cm-1. The baseline of spectra was corrected, and the curve of spectra was smoothened. The surface area was determined with 0.5 g of SB or MB samples using N₂ sorption isotherms run on Macromeritics ASAP 2010, USA. The samples were degassed at 200 °C for 8 h prior to analysis.

Chemical characterization for soil

The soil samples were air-dried and pulverized with an agate mortar to pass a 200 μm (80 mesh) sieve. The cation exchange capacity (CEC) was determined using the sodium acetate method [22]. The pH and electrical conductivity (EC) were measured on a soil slurry with a solid/solution ratio of 1:10, using a calibrated pH meter and EC meter respectively.

Sorption of MB with artificial human urine (AHU)

For the batch sorption experiment, AHU that contains 30 g PO₄³⁻/L was prepared according to the method described by [23] (Table 1). The pH value of AHU was adjusted to the 6.0-6.5 pH range with 1.0 N HCl and 1.0 N NaOH. Stock AHU was stored in a plastic container at 4°C. The AHU stock was warmed to room temperature before being used. Finally, 100 mg of albumin and 4.0 g of creatinine were slowly mixed into the 2.0 L of the AHU solution.

Table 1. Properties and Composition of Artificial Human Urine [23]

Property and Composition	Amount
pH	6.0 - 6.5
Specific gravity (g/mL)	1.020
Osmolality (mOsm/kg)	861
Urea (mM)	416
NaH_2PO_4 (mM)	17.60
NaCl (mM)	154.00
NH ₄ Cl (mM)	48.00
Na ₂ SO ₄ (mM)	21.10

Batch adsorption experiments were conducted by studying the effect of Mg content in MB, MB dosage, contact time, and initial concentration of AHU on adsorption of PO₄³⁻ MB. Various amount of MB (i.e., 0.005, 0.01, 0.05, and 0.10 g) was weight and agitated with 30 mL of stock AHU in 50 mL centrifuge tubes using a rotator at 100 rpm at room temperature for 4 h. Blanks containing AHU without MB were also included in the same experiments. After 4 h of agitation, the residual AHU solutions were filtered with a 0.45 μm syringe filter, and the concentration of PO₄³⁻ was determined by colorimetry using a UV-VIS spectrophotometer and a combined reagent (i.e., potassium antimony tartrate solution, ammonium

molybdate solution, and ascorbic acid solution). Thirteen millilitres of combined reagent were added to 1.0 mL of residual AHU solution in a 25 mL volumetric flask, topped to the mark with DI water, and shaken thoroughly. It was then allowed to stand for 30 min for colour development. The absorbance was measured at 880 nm in a 1-cm quartz cuvette. A calibration curve was prepared by plotting the absorbances of PO₄³⁻ standards with various concentrations and was then used to determine the concentration of PO₄³⁻ in AHU.

The PO₄³⁻ removal percentage and uptake were calculated using equations 1 and 2, respectively. The dosage of MB that gives the highest removal percentage

(i.e., 0.10 g) was chosen for the next sorption experiments.

Removal percentage (% w/w) = $\frac{P_{initial} - P_{final}}{P_{initial}} \times 100 \%$

Uptake,
$$q_e \text{ (mg/g)} = \frac{(P_{initial} - P_{final})V}{M}$$
 (2)

Where $P_{initial}$ and P_{final} (mg/L) are the initial and equilibrium concentrations of PO₄³⁻. V is the volume of the AHU (L), and M is the mass of dry MB (g).

For the sorption isotherm experiment, 10 g of MB were agitated with 30 mL AHU at various PO₄³concentrations (i.e., 66.8, 93.1, 237, 520, 683, 734, 1636, 2472, and 3038 mg/L) in closed 50 mL centrifuge tubes using a rotator at 100 rpm and room temperature for 4 h. For sorption kinetic study, 10 g of MB was agitated at 100 rpm with 30 mL AHU (initial PO₄³concentration 374 mg/L) in a 50 mL centrifuge tube at room temperature for 4 h. All residual AHU solutions were filtered through a 0.45 µm syringe filter, and the concentration of PO₄³⁻ was determined by colorimetry. The PO₄³⁻ uptake by MB was calculated using equation 2 and studied using non-linear Langmuir (Equation 3) and Freundlich (Equation 4) isotherm models as well as non-linear pseudo-first-order (Equation 5) and pseudosecond-order (Equation 6) kinetic models.

Langmuir isotherm model:

$$q_{\rm e} = \frac{q_{\rm max} \cdot K_{\rm L} \cdot C_{\rm e}}{1 + K_{\rm L} \cdot C_{\rm e}} \tag{3}$$

Freundlich isotherm model:

$$q_{\rm e} = K_{\rm F} \cdot C_{\rm e}^{1/\rm n} \tag{4}$$

Where q_e (mg/g) is the PO₄³⁻ uptake, and C_e (mg/L) the concentration of PO₄³⁻ in residual AHU solution at equilibrium. K_L is the equilibrium constant for the Langmuir model. Lastly, K_f [(mg g⁻¹)(mg L⁻¹) ⁿ] is the Freundlich constant that is related to adsorption capacity, and n is the Freundlich constant related to adsorption intensity. Graphs of q_e versus C_e were plotted to determine Langmuir and Freundlich parameters. Then

the parameters were compared to determine the isotherm model that best fit the sorption data.

The pseudo-first-order model:

$$q_{t} = q_{e} \left(1 - e^{-k_{1}t} \right) \tag{5}$$

The pseudo-second-order model:

$$q_{\rm t} = \frac{k_2 \cdot q_e^2 \cdot t}{1 + K_2 \cdot q_e t} \tag{6}$$

Where q_e (mg/g) is the uptake of PO₄³⁻ at equilibrium and q_t (mg/g) is the amount of phosphate from AHU adsorbed at time, respectively. Next, t is the contact time in minutes, and the adsorption rate constants, k_1 (1/min) is the rate constant for the pseudo-first-order model, while k_2 (g/[mg.min]) is the rate constant of the pseudo-second-order model. Parameters for both kinetic models were determined by plotting a graph of q_t (mg/g) versus t (min).

Leaching tests

The leaching test followed the method described by [24] with several modifications. Calcium chloride solution (0.01M, pH = 7) was used to fill up the 50 mL syringe columns that were then irrigated on MB in the syringe column. Lead-contaminated soil was collected from a shooting range located in Universiti Pertahanan Nasional Malaysia (UPNM). The 50 mL syringe columns of MB were irrigated with CaCl₂ using a flow rate that represents the average distribution of rainfall intensity in Peninsular Malaysia (i.e., >10 mm/h) [25]. The total duration of the experiment was 36 h. The leachate produced by each column was sampled in 10 mL volume intervals. The samples were collected in acid-washed 50 mL centrifuge bottles and stored at 3.9 °C until analysis. A tip at the bottom was used to direct the outflow into sampling containers. The 50 mL syringe columns had a diameter of 3.0 cm and were filled with soil and MB to a height of 7.35 cm according to the weight ratio in Table 2. At the bottom of the 50 mL syringe columns, a 1 mm mesh-sized gauze was attached to hold the soil in place. Untreated shooting range soil and ground magnesium limestone (GML)-treated soil

were also subjected to leaching tests as the negative and positive control, respectively.

Modified selective sequential extraction (SSE)

Soil samples were incubated with GML or MB at two application rates of 1.0% w/w and 5.0% w/w (Table 2). Soil samples that were not incubated with any material were compared as control. About 1.0 g of treated soil samples were air-dried, crushed to <2 mm diameter

using an agate mortar, and transferred into 50 mL polypropylene centrifuge tubes. Referring to Table 3, the extraction began from step 1 (exchangeable fraction), until step 5 (residual fraction). The supernatants were separated by centrifugation at 1,400 rpm for 10 min. Each liquid fraction was filtered through a 0.45 µm syringe filter, and the Pb content was determined in each of the five extracts of soil samples using ICP-OES [26].

Table 2. The weight (g) of shooting range soil (Soil), Mg-modified biochar (MB), and ground magnesium limestone (GML) of treated soil samples at 1.0 % (w/w) and 5.0 % (w/w) application rates for leaching test and selective sequestration extraction (SSE) experiments

Soil Amendment	Weight (g)		
	1.0% (w/w)	5.0 % (w/w)	
Control	10.0 g Soil	10.0 g Soil	
MB	9.9 g Soil + 0.1 g MB	9.5 g Soil + 0.5 g MB	
GML	9.9 g Soil + 0.1 g GML	9.5 g Soil + 0.5 g GML	

Table 3. Modified selective sequential extraction procedures

Step	Fraction	Reagent	Conditions
1	Exchangeable (E)	8.0 mL of 1.0 M MgCl ₂ (pH 7)	1 h, 25°C
2	Carbonate (C)	8.0 mL of 1.0 M NaOAc (pH 5)	5 h, 25°C
3	Fe-Mn oxide (FM)	20 mL of 0.04 M NH ₂ OH.HCl in 25% HOAc (v/v)	6 h, 96°C
4	Organic (O)	$3.0 \text{ mL of } 0.02 \text{ M HNO}_3 + 5.0 \text{ mL of } 30\% \text{ H}_2\text{O}_2 \text{ (pH 2)}$	2 h, 85°C
		3.0 mL of 30% H ₂ O ₂	3 h, 85°C
		$5.0 \text{ mL of } 3.2 \text{M NH}_4 \text{OAC} + 20\% \text{ HNO}_3 \text{ (v/v)}$	30 min, 25°C
5	Residual (R)	HNO ₃ -HCl digestion	

Results and Discussion Chemical characterisation for SB, MB, and Spent MB

The elemental composition of SB, MB, and spent MB are shown in Table 4. The overall content of C in SB was relatively low possibly due to the low cellulose content in SD [27]. The pyrolysis process at high temperature (i.e., >500 °C) intensifies the degree of carbonization and increased the C content in SB to 69.03% [28]. Modification with MgO₂ introduced Mg and has slightly decreased C content in MB [29]. Soluble Mg may have been dehydrated to form MgO on the surface of MB [30]. The N content in the Spent MB content after sorption with AHU. Besides the PO₄³⁻, urea is also present in AHU and it is naturally decomposed by microbes to form ammonium ions (NH₄⁺). Possible

precipitation of struvite and its attachment onto the surface of the spent MB exhibited a higher P content [31].

Figures 1 (a), (b), and (c) show the surface of SD, MB, and Spent MB, respectively. The surface of SD was originally smooth with a compact, non-porous structure. Upon pyrolysis, the surface of SB was uneven with more pores formed on its surface and with a much higher C content. A larger pore size was observed in SB compared to that for SD. Pyrolysis at a higher temperature may have allowed more removal of volatile matter from SD and developed a larger pore in SB. The quantity of micropores in SB may have increased in diverse ranges [32]. Meanwhile, The SEM images in Figure 2 show that pores were smaller, and the surface was coarser after SB was modified with MgO₂. The average pore diameter

decreased from 3 nm to 1 nm after the Mg impregnation process due to the blockage of pores in biochar by Mg compounds [33]. Figure 1 (d) shows the presence of PO₄³⁻. Figure 2 further indicates that elemental P was associated with N, and Mg, possibly due to the formation of struvite crystals. The increasing P% in Spent MB coincides with decreasing content of Mg% and C%. The result was predictable as the low content of C% might be due to the phenolic hydroxyl and

carboxylic groups on the surface of Spent MB being preoccupied with PO_4^{3-} and NH_4^+ through the ion exchange mechanism [34]. Both Na and Cl were the most obvious in Figure 2, indicating that NaCl was also co-precipitated with struvite on the surface of Spent MB. Other Mg compounds (i.e., $Mg_3(PO_4)_2$, $MgHPO_4$, or $Mg(H_2PO_4)_2$) may also be present in Spent MB but may be significant in quantity [35].

Table 4. Elemental composition of SD, SB, MB, and Spent MB

Element	Composition			
	SD	SB	MB	Spent MB
С	45.15	69.03	52.08	25.35
O	26.66	3.19	5.37	20.55
Mg	-	-	1.19	0.06
Si	-	-	1.50	0.06
Ca	0.00	0.00	2.36	0.22
S	0.00	0.00	1.77	1.41
N	28.19	27.78	2.27	17.35
C1	0.00	0.00	0.00	33.89
P	0.00	0.00	0.00	1.11
Au	-	-	33.46	-

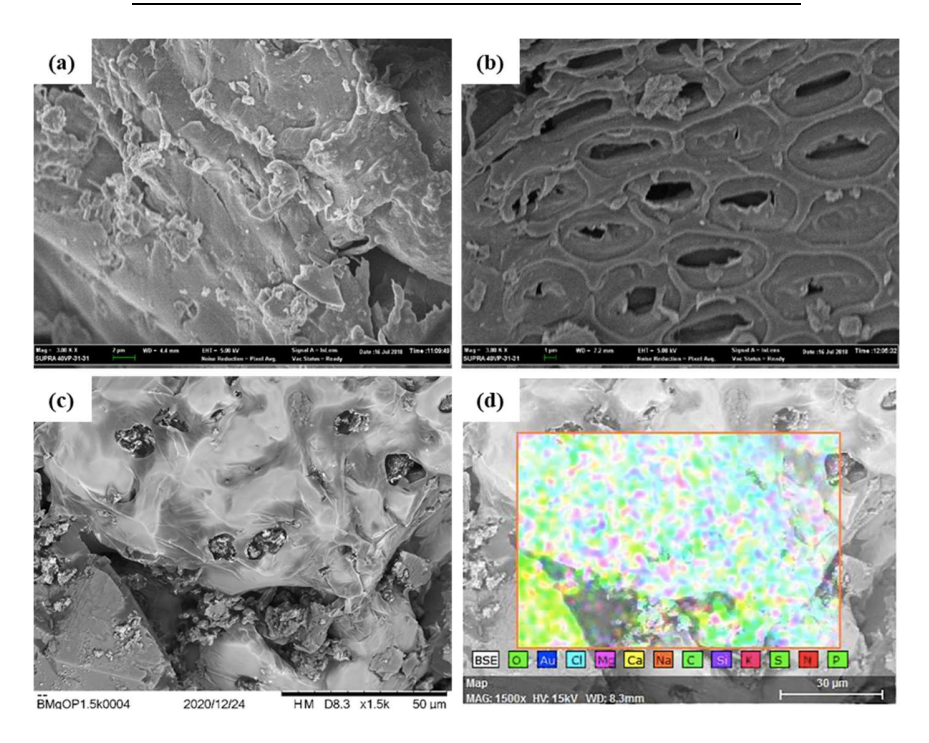


Figure 1. Scanning electron micrograph (SEM) images of (a) sawdust (SD), (b) Mg-modified biochar (MB), (c) Spent MB, and (d) combined elemental map for Spent MB

Yong et al.: RECOVERY OF PHOSPHATE FROM ARTIFICIAL HUMAN URINE USING MAGNESIUM-MODIFIED BIOCHAR FOR IMMOBILIZATION OF LEAD IN SOIL

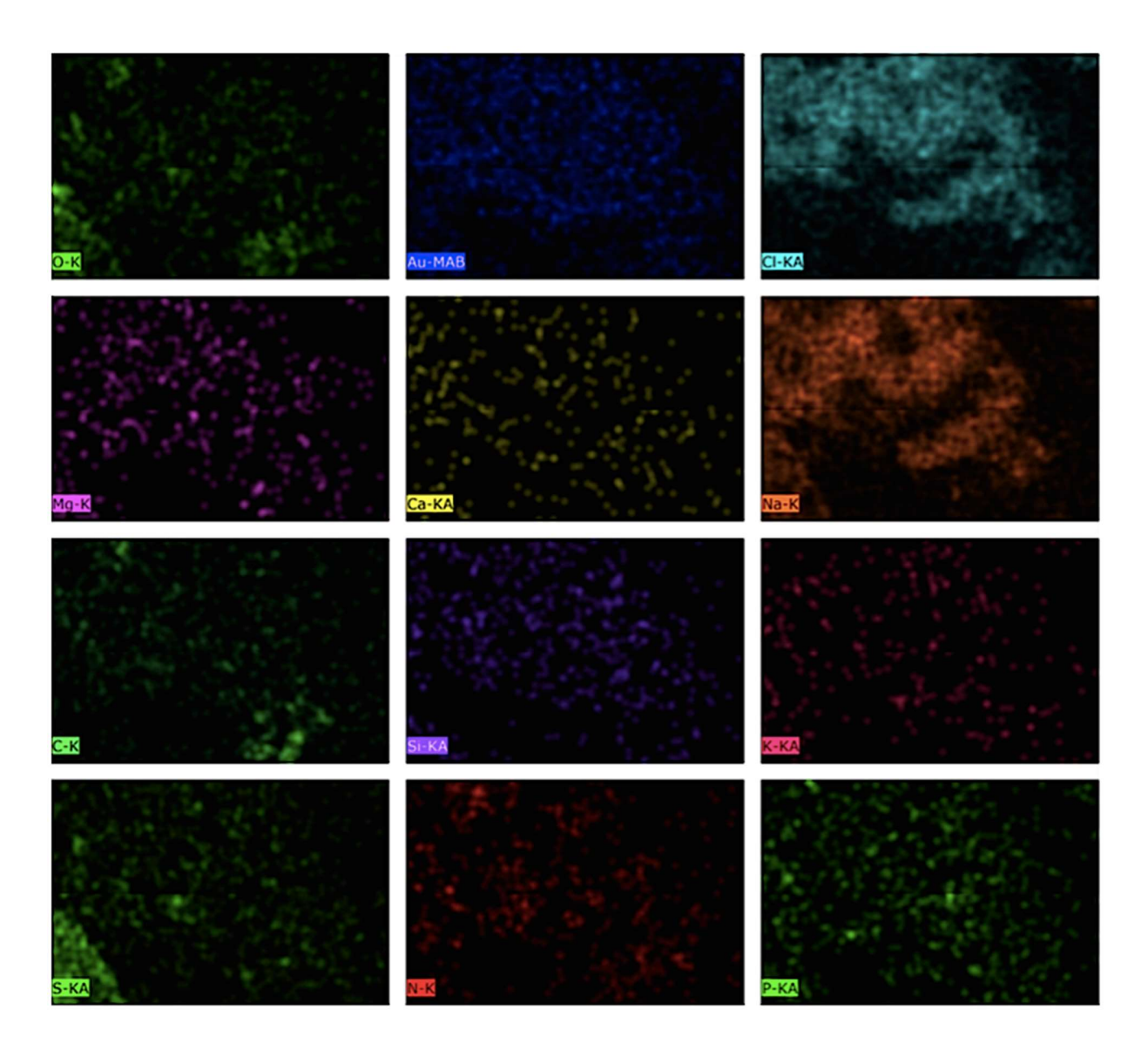


Figure 2. Elemental map of O, Au, Cl, Mg, Ca, Na, C, Si, K, S, N, and P for Spent MB

The BET surface areas and pore width of SB and MB are shown in Table 5. The high pyrolysis temperature at 700 °C allowed the formation of porous SB with a high BET surface area (145 m^2/g). This could be due to the formation of micropores when the pyrolysis temperature is greater than 500 °C [36]. Pyrolysis at a high temperature removed the volatile matter and poreblocking tar from SD, leading to the greater formation of micropores and an increase in the BET surface area and pore volume [37]. However, the modification process with MgO₂ has also decreased the BET surface

area value from 145 m²/g to 5.05 m²/g. This could be due to the excessive chemical oxidation by MgO₂ that converts micropore to macropore in MB [38]. The increase in average pore width (nm) in MB corroborates this hypothesis. The possible formation of Mg nanoparticle in the inner pores of MB may also cause blockage and leads to a decrease in the BET surface area [39]. During the dehydration process of MB, a higher amount of Mg concentration leads to Mg becoming hydrated thus forming an excess MgO that blocks the pores of MB [40].

Table 5. The BET surface areas (m²/g), average pore width (nm), and CEC of sawdust biochar (SB) and Mg-modified biochar (MB), and Spent MB

Parameter	SB	MB	Spent MB
BET surface area (m ² /g)	145	5.05	-
Average pore width (4V/A) (nm)	11.62	14.88	-
CEC (cmol/kg)	0.757	1.034	1.015

The CEC values for SB, MB, and Spent MB are shown in Table 5. Modification of MB with MgO₂ marginally increased CEC values from 0.7569 cmol/kg to 1.034 cmol/kg. The CEC value for Spend MB (1.015 cmol/kg) is also similar to that of MB. The surface of MB may have been slightly oxidized by MgO₂. The insignificant increase in CEC value may also be due to a possible formation of a strong Mg-O bond that prevents deprotonation of the polar functional groups. Similarly, a potential PO₄³⁻ adsorption and precipitation of struvite did not cause further oxidation and the amount of polar functional group remains the same as that of MB. The formation of struvite may have occupied the pores and neutralized the negative charge of the polar functional groups on the surface of MB [41].

Figure 3 illustrates the vibration bands for SB, MB, and Spent MB. The hydroxyl group (-OH) is present in

cellulose, hemicelluloses, and lignin which is also responsible for the binding of Mg [42]. The hydroxyl band is not observed in SB, where there was a possibility that most of the cellulose, hemicellulose and lignin degraded due to the high pyrolysis temperature. The vibration bands at 828 cm⁻¹ are related to the aromatic C-H in MB, indicating that the added Mg was adsorbed [43]. The presence of the NH₄⁺ band is shown at 1463 cm⁻¹-1465 cm⁻¹ [44]. Furthermore, the NH₂ stretching bands for spent MB are shown at 3453 cm⁻¹. Bands at 1090-1096 cm⁻¹ were due to the P-O stretching vibration of PO₄³⁻ [45]. Bands at 1641-1674 cm⁻¹ are the stretching vibrations for C=O carboxylate (1641 cm⁻¹) and C=O amide (1674 cm⁻¹). The wavenumber at 1389-1467 cm⁻¹ corresponds to the sp3 C-H bending vibration [46]. The presence of phenolate (1300 cm⁻¹) along with carboxylate and amide were mainly involved in the Mg and PO₄³- adsorption.

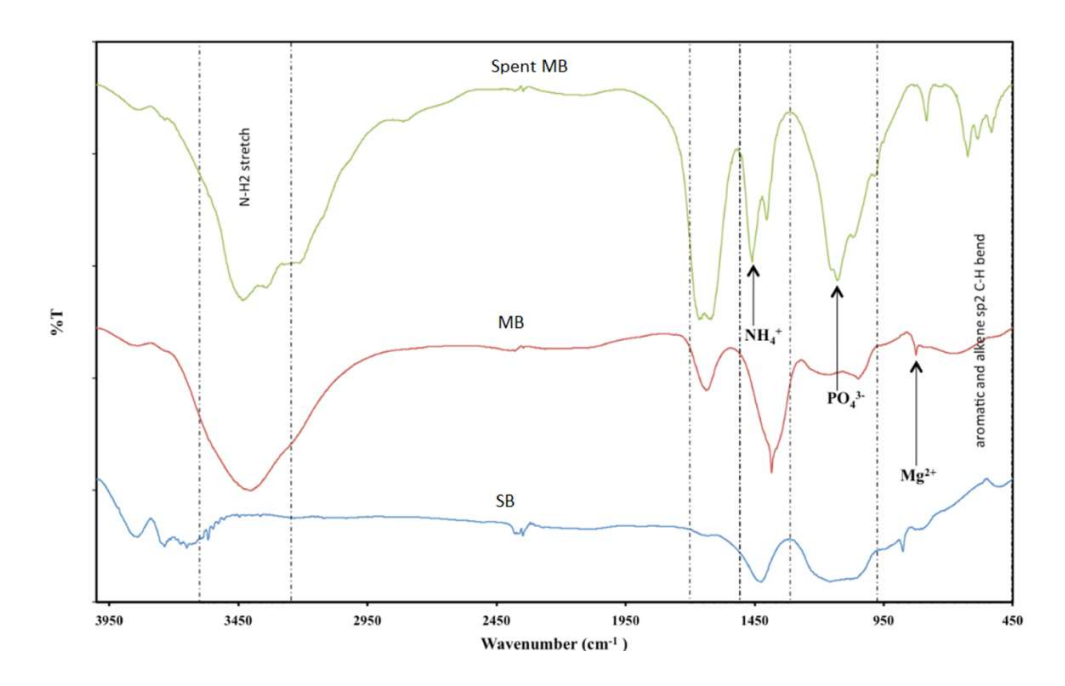


Figure 3. Stacked FTIR spectra of sawdust biochar (SB), Mg-modified biochar (MB), and Spent MB

Figure 4 shows the TG and derivative curve (DTG) thermogram of SD, MB, and Spent MB. Thermal decomposition was characterized by four different mass loss phase that has been separated by the lines for specific temperature intervals. The first decomposition stage happened to all the samples at < 300 °C. Partial decrease in total mass was observed, possibly due to the evaporation of water, and minor de-volatilization [47]. The weight loss that took place between 300 and 500 °C refers to the degradation of cellulose [48]. There were two decomposition stages between 250 °C and 350 °C at phase 2 that correspond to the sharp peak of DTG at 350 °C for MB. This indicated that the first

decomposition was due to the weight loss of residual water, while the second decomposition stage could be due to the degradation of the Mg hydrates along with the third stage showing a formation of magnesium hydroxychloride (MgOHCl) [49]. Meanwhile, the second phase for Spent MB showed no peak with a flat decomposition stage starting at 250 °C. This could be due to the bonding of PO₄³⁻ from AHU. The Mg²⁺ ion forms struvite and this may lead to the absence of free MgCl₂ hydrates. Lastly, stage 3 and 4 thermal decompositions at 450 °C and 800 °C, respectively were attributed to the slow decomposition of residual solids that contributed to the formation of char [50].

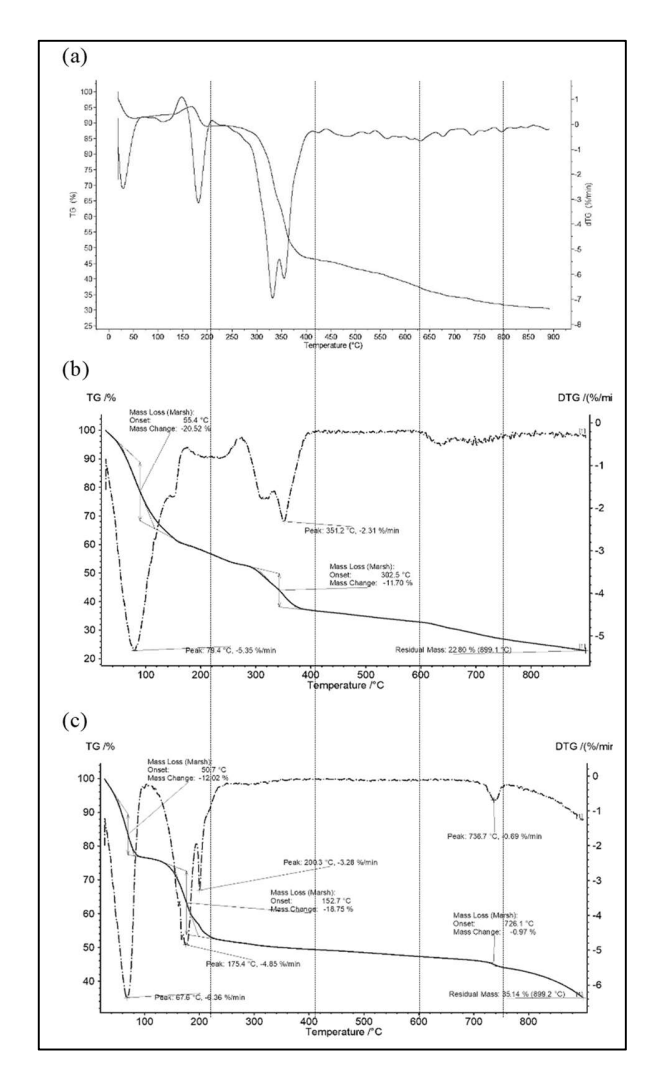


Figure 4. TGA and DTG of (a) sawdust (SD), (b) Mg-modified biochar (MB), and (c) spent MB at heating rate of 3°C/min

Batch sorption of PO₄³⁻ from AHU: Effect of initial concentration of PO₄³⁻

The PO₄³⁻ sorption capacities of MB increased from 668 mg/g to 9554 mg/g when the initial PO₄³⁻ concentrations of AHU were increased from 6.68 mg/L to 304 mg/L. A higher concentration allows greater diffusion rates and contact of PO₄³⁻ in the aqueous phase with the surface of MB. Thus, more PO₄³⁻ can bind with polar functional

groups and increase sorption capacity [51]. Adsorption isotherm parameters in Table 6 show that the PO_4^{3-} adsorption of MB fits better with the Freundlich model (i.e., $R^2 = 0.827$) [52]. This shows that adsorption of PO_4^{3-} occurred on heterogeneous active sites on the surface of MB. The Langmuir maximum sorption capacity for MB was 8967 mg/g.

Table 6. Parameters of isotherm (Langmuir and Freundlich) and kinetic models (pseudo-first-order and pseudo-second-order) of PO₄³⁻ sorption by MB

Isotherm Model	Isotherm Models Langmuir		Kinetic Models Pseudo-first-order		
Langmuir					
$q_{ m max} ({ m mg/g})$	8967	k ₁ (g/[mg.min])	0.053		
$K_{\rm L}$ (L/mg)	0.029	$q_{\rm e}({ m mg/g})$	114.5		
R^2	0.773	R^2	0.850		
Freundlich		Pseudo-second-order			
K_{F}	944	k ₂ (g/[mg.min])	0.0762		
n	2.456	$q_{\rm e}({ m mg/g})$	9.937		
\mathbb{R}^2	0.827	R^2	0.903		

Effect of contact time on uptake of PO₄³-(mg/g)

The uptake of PO₄³⁻ by MB reached the first equilibrium in the 10th minute with PO₄³ uptake of 81.1 mg/g. The second sorption equilibrium was observed in the 75th minute with a PO₄³⁻ uptake of 127 mg/g. The surface sites for binding PO₄3- become limited and saturated when contact time was prolonged to two hours [53]. Removal of PO₄³⁻ from AHU may be higher if contact time is allowed to extend for a month. Precipitation and crystallization of Mg minerals may take place. Moreover, MB has an enhancement of negative-charged polar functional groups on its surface, and the main sorption sites for magnesium (i.e., phenolic and carboxyl groups) were deprotonated to allow free Mg²⁺ ions to precipitate as MgO [54]. Kinetic parameters of PO₄³⁻ sorption data analysed using non-linearised pseudo-first-order and pseudo-second-order models for MB are shown in Table 9. Adsorption of PO₄³⁻ occurred rapidly within 15 min of contact time with more than 70 mg/g of uptake. The PO₄3- adsorption by MB was better described by the pseudo-second-order kinetic model with a higher correlation coefficient (i.e., 0.903) than that of the pseudo-first-order model (i.e., 0.85). This outcome suggests that the adsorption process may

involve the formation of strong chemical bonds between PO₄³⁻ and the polar functional group on the surface of MB [55].

Modified selective sequential extraction

Figure 5 illustrates the percentage of Pb in the five fractions of the selective sequential extraction (SSE) for soils incubated with GML, and spent MB at 1 and 5% w/w application rate. The first fraction is the exchangeable Pb that easily reacts with the ionic content in water and becomes soluble [56]. This form of Pb is considered available and may cause adverse effects on living organisms. The percentage of exchangeable Pb (first fraction of the SSE procedure) is shown in Figure 6. Exchangeable Pb in unamended soil was the highest (0.33%). Complete immobilization of exchangeable Pb (0 %) was achieved by treating the soil with 0.5 g of spent MB (5% w/w MB). Soil treated with spent MB has a decrease of Pb in fraction 1, but an increase in fractions 2 and 3. This shows that Pb was converted to a relatively less available form that is not readily taken up by plants [34]. This could be due to the chemical reaction between soluble Pb²⁺ ions with PO₄³⁻ from spent MB, forming the insoluble Pb minerals such as Pb₃(PO₄)₂.

The second fraction generally refers to the Pb that is likely to bind with carbonate and is susceptible to pH alterations. Immobilization of Pb in the carbonate fraction could be due to the bonding with hydroxide ions, and the precipitation process of Pb with PO₃⁻⁴ or CO₂⁻³ that were abundant in spent MB [57]. According to Tessier [26], a decrease of soil pH to 5.0 in the second fraction would solubilize Pb which is particularly adsorbed in the carbonate-bound fraction. In this study, spent MB was alkaline with a pH value of 12. The alkaline nature was due to the presence of struvite and alkaline minerals in spent MB which includes hydroxides and oxides of potassium and calcium [58]. For high Pb in fraction 4 (i.e., bound to organic matter), Tessier reported that some organic matter may

eventually be released into the environment as biomass may deteriorate, causing it to release the soluble Pb under certain oxidizing conditions in natural waters [26]. Fortunately, the biochar component in the spent MB is more stable than biomass and this was proven as treatment of 1 and 5% w/w of Spent MB gave the least percentage of Pb in fractions 4 of 7.3 % and 12.7 %, respectively. This may be due to the less complexation of Pb with the stable organic structure with struvite bound to MB. Most of the exchangeable Pb were probably precipitated with struvite and ash originated from SB. This shows that treatment of shooting range soil with Spent MB promoted Pb immobilization and minimizes the health risk [59].

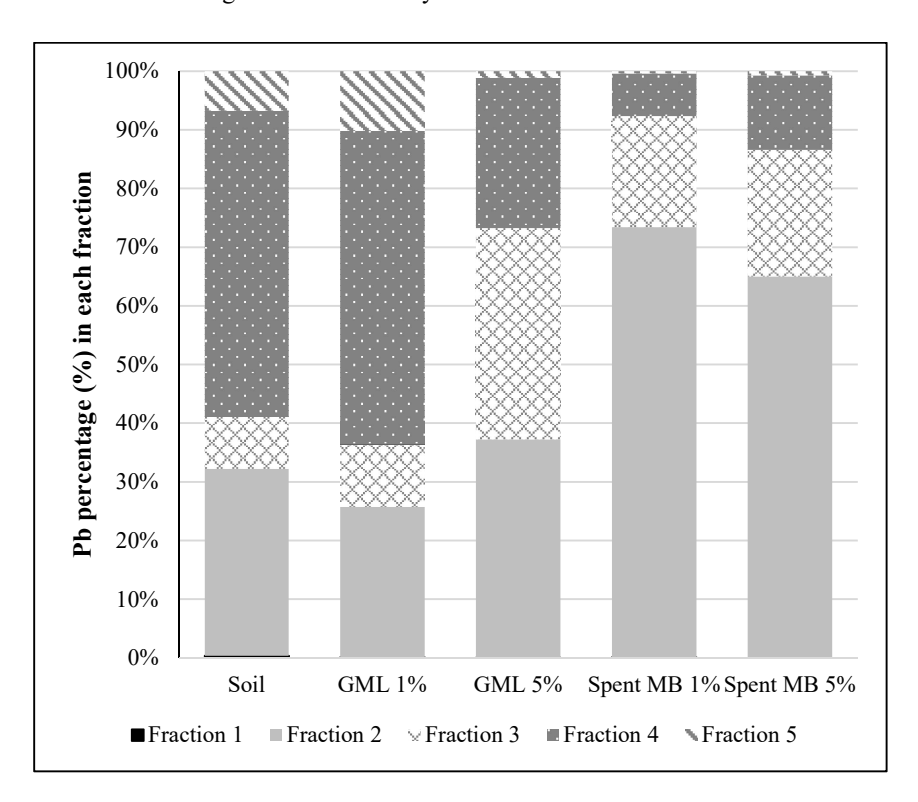


Figure 5. Percentage of lead (Pb) (% w/w) in fractions of the selective sequential extraction experiment for soil treated with GML and spent MB at 1 and 5 % w/w application rate.

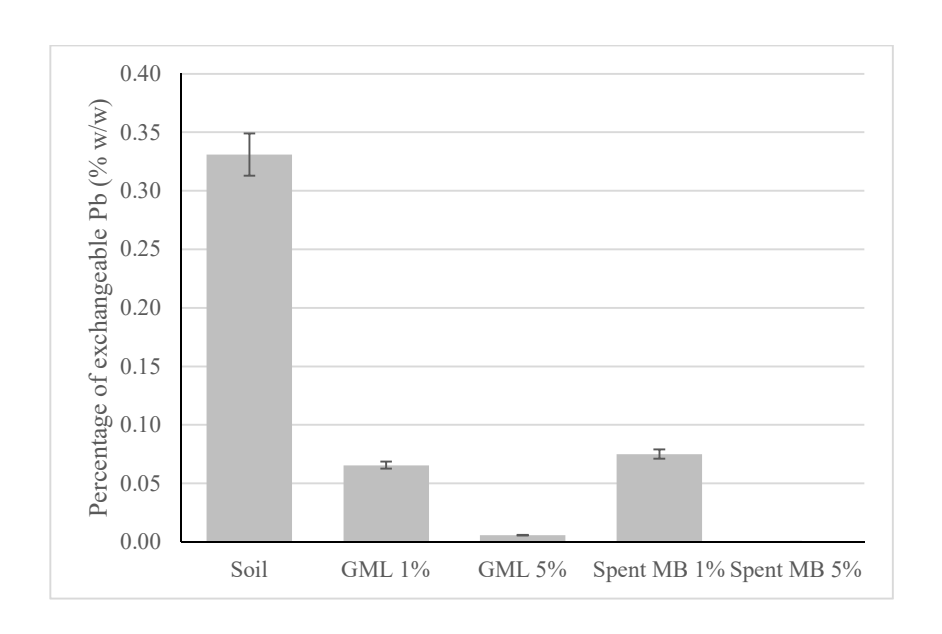


Figure 6. Percentage of exchangeable lead (Pb) (% w/w) for soil treated with ground magnesium lime (GML), and spent modified biochar (MB) at 1 and 5 % w/w application rate.

Leaching rate of Pb from soils modified with Spent MB, and Ground Magnesium Lime (GML)

Figure 7 shows the variations in the available Pb concentration of leachates from soils treated with MB and GML over the volume of 0.01M CaCl₂. For the untreated soil column, the concentration of Pb in leachate had increased slightly during the initial stage of the leaching process. The concentration of Pb drastically increased until it reached the maximum Pb concentration of 5.96 mg/L. Then, the Pb concentration decreased gradually to 2.40 mg/L. The overall trend for soil column leaching was gradually decreased from high

concentrations of Pb compared to other samples. However, the Pb concentration in leachates coming from soil columns treated with GML and Spent MB were similar and remained constant below 1.63 mg/L. This shows that amendment with MB can mitigate Pb leaching from soil and the performance is comparable to the commercial liming agent of GML. The mechanism of Pb immobilization by struvite-modified magnesium biochar can be explained by the dissolution of PO_4^{3-} to the aqueous phase followed by the precipitation process of hydroxypyromorphite $Pb_{10}(PO_4)_6(OH)_2$ [60]. The reaction equation is represented as follows:

 $MgNH_4PO_4 \cdot 6H_2O + 2H + \\ \leftrightarrow Mg^{2+} + NH_4^+ + H_2PO_4 + 6H_2O + 10Pb^{2+} + 6H_2PO_4 + 2H_2O \\ \leftrightarrow Pb_{10}(PO_4)_6(OH)_2 \\ \downarrow \\ + 14H^+ + Pb^{2+} + HPO_4^{2-} \\ \leftrightarrow PbHPO_4 \\ \downarrow$

Yong et al.: RECOVERY OF PHOSPHATE FROM ARTIFICIAL HUMAN URINE USING MAGNESIUM-MODIFIED BIOCHAR FOR IMMOBILIZATION OF LEAD IN SOIL

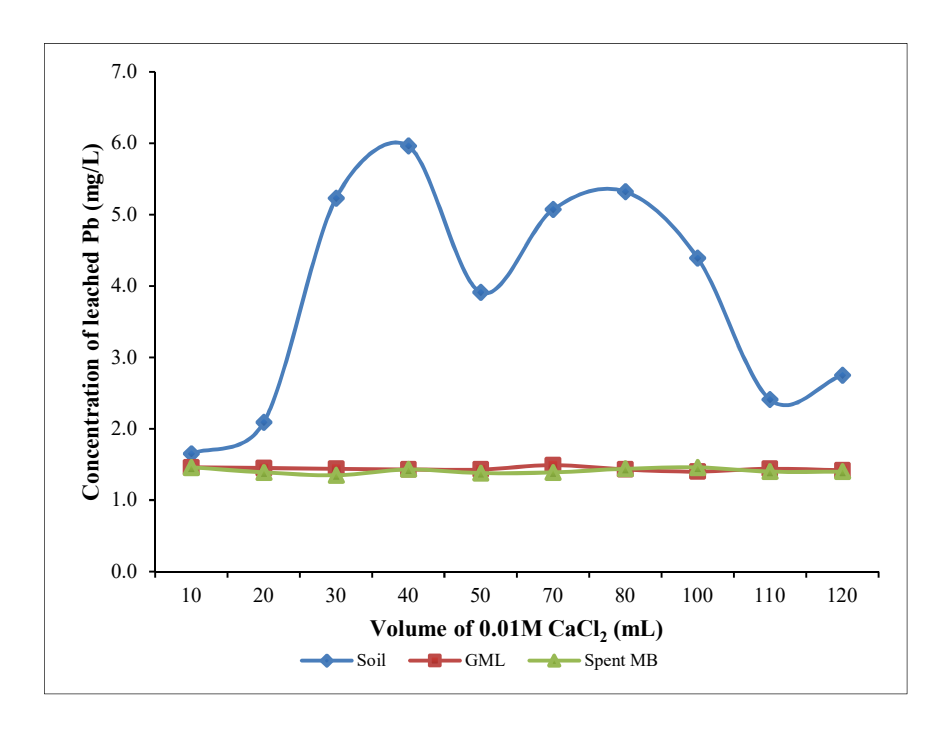


Figure 7. The concentration of Pb in leachates (mg/L) as a function of the volume of 0.01 M CaCl₂ solution of soil columns treated with 1 % w/w Spend MB, ground magnesium lime (GML).

Conclusion

This research exhibited the application of SB, MB, and Spent MB as adsorbents because of their features that were easily available, not harmful to the environment, its oxygenated functional groups on biochar surfaces, and the potential for higher sorption capacity. The modification process of MgO₂ seemed able to improve PO₄³- uptake of SB. The SEM-EDX analysis showed that pyrolysis has helped develop macropores in SB and is still retained MB after modification with MgO₂. However, due to possible over oxidation, the microporous structure of MB was not retained. Fortunately, the modifications with MgO2 led to additional negative-charged polar functional groups for the adsorption of Mg and the subsequent PO₄³- from AHU. Although struvite crystal was successfully precipitated from AHU using MB, a significant amount of NaCl was also present in the Spent MB. Long-term application of Spent MB may introduce Na and may damage soil structure due to an increase in salinity. Even so, Spent MB has shown greater potential to immobilize Pb in soil than GML. Based on the batch adsorption study, modification of MgO2 has produced MB with a high Langmuir maximum sorption capacity for PO₄³-(i.e., 8967 mg/g), and is higher than that of biochar modified with only MgCl₂ (i.e., 8026 mg/g) [61]. Adsorption isotherm analysis indicated that the uptake of PO₄3- by MB was best described by the Freundlich model, with an assumption that several layers of adsorption mechanism occurred on a heterogeneous surface of MB. Kinetic study results suggested that the entire adsorption process for MB was dominated by the chemisorption process via an ion-exchange mechanism. While the small amount of Mg did have some significant effect on adsorption of PO₄³⁻ onto MB. Lastly, the Pb immobilization test results for the three samples have Spent MB indicated that exhibited immobilization ability for Pb compared to soil with GML. Thus, amendment with the Mg-impregnated biochar can mitigate Pb leaching from soil to improve PO₄³- utilization.

Acknowledgement

Authors acknowledge the Universiti Teknologi MARA for funding under the Geran Penyelidikan Khas (600-RMC 5/3/GPK (093/2020).

References

- Mackey, K. R. M. and Paytan, A. (2009). Phosphorus cycle. Encyclopedia of Microbiology, Academic Press, Cambridge, Massachusetts, USA: pp 322-334.
- Department of Environment Malaysia (2009). Environmental Quality (Industrial Effluent) Regulations, Ministry of Science, Technology and Environment, Kuala Lumpur.
- Sedlak, R. (2018). Phosphorus and nitrogen removal from municipal wastewater: principles and practice. Routledge, New York, USA: pp 1-256.
- 4. Rittmann, B. E., Mayer, B., Westerhoff, P. and Edwards, M. (2011). Capturing the lost phosphorus. *Chemosphere*, 84(6): 846-853.
- Sakulpaisan, S., Vongsetskul, T., Reamouppaturm, S., Luangkachao, J., Tantirungrotechai, J. and Tangboriboonrat, P. (2016). Titania-functionalized graphene oxide for an efficient adsorptive removal of phosphate ions. *Journal of Environmental Management*, 167: 99-104.
- Yin, H., Kong, M. and Fan, C. (2013). Batch investigations on P immobilization from wastewaters and sediment using natural calcium rich sepiolite as a reactive material. Water Research, 47(13): 4247-4258.
- 7. Sohi, S. P. (2012). Carbon storage with benefits. *Science*, 338(6110): 1034-1035.
- Ghorbani-Khosrowshahi, S. and Behnajady, M. (2016). Chromium(VI) adsorption from aqueous solution by prepared biochar from *Onopordom heteracanthom*. *International Journal of Environmental Science and Technology*, 13: 1803-1814
- 9. Tan, Z., Lin, C., Ji, X. and Rainey, T. (2017). Returning biochar to fields: A review. *Applied Soil Ecology*, 116: 1-11.
- He, Y., Zhou, X., Jiang, L., Li, M., Du, Z., Zhou, G., Shao, J., Wang, X., Xu, Z., Hosseini Bai, S., Wallace, H. and Xu, C. (2017). Effects of biochar application on soil greenhouse gas fluxes: a meta-analysis. GCB Bioenergy, 9(4): 743-755.
- Ab Malek, N. A., Ibrahim, M. L. and Yong, S. K. (2020). Composite biochar derived from palm kernel shells and blood cockle shells for

- immobilizing lead in shooting range soil. *Malaysian Journal of Chemistry*, 22(2): 89-97.
- Almanassra, I. W., McKay, G., Kochkodan, V., Ali Atieh, M. and Al-Ansari, T. (2021). A state of the art review on phosphate removal from water by biochars. *Chemical Engineering Journal*, 409: 128211.
- Alling, V., Hale, S. E., Martinsen, V., Mulder, J., Smebye, A., Breedveld, G. D. and Cornelissen, G. (2014). The role of biochar in retaining nutrients in amended tropical soils. *Journal of Plant Nutrition* and Soil Science, 177(5): 671-680.
- 14. Qiu, M., Liu, L., Ling, Q., Cai, Y., Yu, S., Wang, S., Fu, D., Hu, B. and Wang, X. (2022). Biochar for the removal of contaminants from soil and water: a review. *Biochar*, 4(19): 1-25.
- 15. Xu, K., Zhang, C., Dou, X., Ma, W. and Wang, C. (2019). Optimizing the modification of wood waste biochar via metal oxides to remove and recover phosphate from human urine. *Environmental Geochemistry and Health*, 41(4): 1767-1776.
- Shih, K. and Yan, H. (2016) Chapter 26 The crystallization of struvite and its analog (K-Struvite) from waste streams for nutrient recycling. environmental materials and waste. Academic Press, Cambridge, Massachusetts, USA: pp. 665-686.
- Kloss, S., Zehetner, F., Dellantonio, A., Hamid, R., Ottner, F., Liedtke, V., Schwanninger, M., Gerzabek, M. H. and Soja, G. (2012). Characterization of slow pyrolysis biochars: Effects of feedstocks and pyrolysis temperature on biochar properties. *Journal of Environmental Quality*, 41(4): 990-1000.
- Bakshi, S., Banik, C. and Laird, D. A. (2020). Estimating the organic oxygen content of biochar. Scientific Reports, 10(1): 13082.
- Jung, K. W., Hwang, M. J., Ahn, K. H. and Ok, Y. S. (2015). Kinetic study on phosphate removal from aqueous solution by biochar derived from peanut shell as renewable adsorptive media. *International Journal of Environmental Science and Technology*, 12(10): 3363-3372.

- Fidel, R. B., Laird, D. A., Thompson, M. L. and Lawrinenko, M. (2017). Characterization and quantification of biochar alkalinity. *Chemosphere*, 167: 367-373.
- Tan, Z., Qiu, J., Zeng, H., Liu, H. and Xiang, J. (2011). Removal of elemental mercury by bamboo charcoal impregnated with H₂O₂. Fuel, 90(4): 1471-1475.
- 22. Yong, S. K., Mohd Zin, S. N. and Mad Ariff, M. J. (2016). Effects of rain pH, soil organic matter, cation exchange capacity and total lead content in shooting range soil on the concentration of lead in leachate. *Malaysian Journal of Analytical Sciences*, 20(5): 1066-1072.
- Chutipongtanate, S. and Thongboonkerd, V. (2010). Systematic comparisons of artificial urine formulas for in vitro cellular study. *Analytical Biochemistry*, 402(1): 110-112.
- 24. Iqbal, H., Garcia-Perez, M. and Flury, M. (2015). Effect of biochar on leaching of organic carbon, nitrogen, and phosphorus from compost in bioretention systems. *Science of The Total Environment*, 521-522: 37-45.
- Varikoden, H., Samah, A. A. and Babu, C. A. (2010). Spatial and temporal characteristics of rain intensity in the peninsular Malaysia using TRMM rain rate. *Journal of Hydrology*, 387(3-4): 312-319.
- Tessier, A., Campbell, P. G. C. and Bisson, M. (1979). Sequential extraction procedure for the speciation of particulate trace metals. *Analytical Chemistry*, 51(7): 844-851.
- 27. Chun, Y., Sheng, G., Chiou, C. T. and Xing, B. (2004). Compositions and sorptive properties of crop residue-derived chars. *Environmental Science & Technology*, 38(17): 4649-4655.
- Chen, Y., Yang, H., Wang, X., Zhang, S. and Chen, H. (2012). Biomass-based pyrolytic polygeneration system on cotton stalk pyrolysis: influence of temperature. *Bioresource Technology*, 107: 411-418.
- Li, R., Wang, J. J., Zhou, B., Ali, M. K. A. A., Zhang, Z., Gaston, L. A., Lahori, A. H., Mahar, A. (2016). Enhancing phosphate adsorption by Mg/Al layered double hydroxide functionalized biochar with different Mg/Al ratios. Science of the Total Environment, 559: 121-129.

- Li, R., Wang, J. J., Zhou, B., Zhang, Z., Liu, S., Lei, S., Xiao, R. (2017). Simultaneous capture removal of phosphate, ammonium and organic substances by MgO impregnated biochar and its potential use in swine wastewater treatment. *Journal of Cleaner Production*, 147: 96-107.
- 31. Thant Zin, M. M. and Kim, D.-J. (2021). Simultaneous recovery of phosphorus and nitrogen from sewage sludge ash and food wastewater as struvite by Mg-biochar. *Journal of Hazardous Materials*, 403: 123704.
- 32. Xi, J., Li, H., Xi, J., Tan, S., Zheng, J. and Tan, Z. (2020). Preparation of high porosity biochar materials by template method: A review. *Environmental Science and Pollution Research*, 27(17): 20675-20684.
- 33. Chen, Q., Qin, J., Cheng, Z., Huang, L., Sun, P., Chen, L. and Shen, G. (2018). Synthesis of a stable magnesium-impregnated biochar and its reduction of phosphorus leaching from soil. *Chemosphere*, 199: 402-408.
- 34. Gong, Y. P., Ni, Z. Y., Xiong, Z. Z., Cheng, L. H. and Xu, X. H. (2017). Phosphate and ammonium adsorption of the modified biochar based on *Phragmites australis* after phytoremediation. *Environmental Science and Pollution Research*, 24(9): 8326-8335.
- Cui, L., Pan, G., Li, L., Bian, R., Liu, X., Yan, J., Quan, G., Ding, C., Chen, T., Liu, Y., Liu, Y., Yin, C., Wei, C., Yang, Y. and Hussain, Q. (2016). Continuous immobilization of cadmium and lead in biochar amended contaminated paddy soil: A five-year field experiment. *Ecological Engineering*, 93: 1-8.
- Tang, J., Zhu, W., Kookana, R. and Katayama, A. (2013). Characteristics of biochar and its application in remediation of contaminated soil. *Journal of Bioscience and Bioengineering*, 116(6): 653-659.
- 37. Angın, D. (2013). Effect of pyrolysis temperature and heating rate on biochar obtained from pyrolysis of safflower seed press cake. *Bioresource Technology*, 128: 593-597.

- 38. Yong, S. K., Bachmann, R. T. and Amin, S. (2020). Oxidised biochar from palm kernel shell for ecofriendly pollution management. *Scientific Research Journal*, 17(2): 45-60.
- 39. Fang, C., Zhang, T., Li, P., Feng, J., R., and Wang, C. (2014). Application of magnesium modified corn biochar for phosphorus removal and recovery from swine wastewater. *International Journal of Environmental Research and Public Health*, 11(9): 9217-9237.
- 40. Huang, Q., Lu, G., Wang, J. and Yu, J. (2011). Thermal decomposition mechanisms of MgCl₂·6H₂O and MgCl₂·H₂O. *Journal of Analytical and Applied Pyrolysis*, 91(1): 159-164.
- 41. Bourke, J., Manley-Harris, M., Fushimi, C., Dowaki, K., Nunoura, T., and Antal., M. J. (2007). Do all carbonized charcoals have the same chemical structure? 2. A model of the chemical structure of carbonized charcoal. *American Chemical Society*, 46(18): 5954-5967.
- 42. Munajad, A., Subroto, C. and Suwarno (2018). Fourier transform infrared (FTIR) spectroscopy analysis of transformer paper in mineral oil-paper composite insulation under accelerated thermal aging. *Energies*, 11(2): 364.
- 43. Novais, S. V., Zenero, M. D. O., Tronto, J., Conz, R. F. and Cerri, C. E. P. (2018). Poultry manure and sugarcane straw biochars modified with MgCl₂ for phosphorus adsorption. *Journal of Environment Management*, 214: 36-44.
- 44. Jing, H. P., Wang, X., Xia, P. and Zhao, J. (2019). Sustainable utilization of a recovered struvite/diatomite compound for lead immobilization in contaminated soil: Potential, mechanism, efficiency, and risk assessment. *Environtal Science Pollution Research*, 26(5): 4890-4900.
- 45. Chauchan, C. K., Joseph, K. C., Parekh, B. B. and Joshi, M. J. (2008). Growth and characterization of Struvite crystals. *Indian Journal of Pure and Applied Physics*, 46: 507-512.
- 46. Khan, S. A., Khan, S. B., Khan, L. U., Farooq, A., Akhtar, K. and Asiri, A. M. (2019). Fourier transform infrared spectroscopy: Fundamentals and application in functional groups and nanomaterials

- characterization. Handbook of Materials Characterization. Springer, Cham: pp. 317-344.
- 47. Hu, M., Chen, Z., Wang, S., Guo, D., Ma, C., Zhou, Y., Chen, J., Laghari, M., Fazal, S., Xiao, B., Zhang, B. and Ma, S. (2016). Thermogravimetric kinetics of lignocellulosic biomass slow pyrolysis using distributed activation energy model, Fraser—Suzuki deconvolution, and iso-conversional method. *Energy Conversion and Management*, 118: 1-11.
- 48. Zhou, C., Yang, W. and Blasiak, W. (2013). Characteristics of waste printing paper and cardboard in a reactor pyrolyzed by preheated agents. Fuel Processing Technology, 116: 63-71.
- 49. Zhang, M., Gao, B., Yao, Y., Xue, Y. and Inyang, M. (2012). Synthesis of porous MgO-biochar nanocomposites for removal of phosphate and nitrate from aqueous solutions. *Chemical Engineering Journal*, 210: 26-32.
- Kim, J. A., Vijayaraghavan, K., Reddy, D. H. K. and Yun, Y.-S. (2018). A phosphorus-enriched biochar fertilizer from bio-fermentation waste: A potential alternative source for phosphorus fertilizers. *Journal of Cleaner Production*, 196: 163-171.
- Haddad, K., Jellali, S., Jeguirim, M., Ben Hassen Trabelsi, A. and Limousy, L. (2018). Investigations on phosphorus recovery from aqueous solutions by biochars derived from magnesium-pretreated cypress sawdust. *Journal of Environmental Management*, 216: 305-314.
- 52. Vijayakumar, G., Tamilarasan, R. and Dharmendirakumar, M. (2012). Adsorption, kinetic, equilibrium and Thermodynamic studies on the removal of basic dye Rhodamine-B from aqueous solution by the use of natural adsorbent perlite. *Journal of Material Environmental Science*, 3(1): 157-170.
- 53. Wang, Z., Shen D., Shen F. and Li, T. (2016). Phosphate adsorption on lanthanum loaded biochar. *Chemosphere*, 150: 1-7.
- 54. Wang, B., Lehmann, J., Hanley, K., Hestrin, R. and Enders, A. (2016). Ammonium retention by oxidized biochars produced at different pyrolysis temperatures and residence times. *RSC Advances*, 6(48): 41907-41913.

- 55. Ho, Y. S. and McKay, G. (2000). The kinetics of sorption of divalent metal ions onto sphagnum moss peat. *Water Research*, 34(3): 735-742.
- Shen, Z., Zhang, Y., Jin, F., McMillan, O. and Al-Tabbaa, A. (2017). Qualitative and quantitative characterisation of adsorption mechanisms of lead on four biochars. *Science of The Total Environment*, 609: 1401-1410.
- 57. Xue, Y., Gao, B., Yao, Y., Inyang, M., Zhang, M., Zimmerman, A. R. and Ro, K. S. (2012). Hydrogen peroxide modification enhances the ability of biochar (hydrochar) produced from hydrothermal carbonization of peanut hull to remove aqueous heavy metals- Batch and column tests. *Chemical Engineering Journal*, 200-202: 673-680.
- Novak, J. M., Lima, I., Xing, B., Gaskin, J. W., Steiner, C., Das, K. C., Ahmedna, M., Rehrah, D., Watts, D. W., Busscher, W. J. and Schomberg, H. (2009). Characterization of designer biochar

- produced at different temperatures and their effects on a loamy sand. *Annals of Environmental Science*, 3: 195-206.
- 59. Wang, H., Wang, X., Li, J., Jing, H., Xia, S., Liu, F. and Zhao, J. (2018). Comparison of palygorskite and struvite supported palygorskite derived from phosphate recovery in wastewater for *in-situ* immobilization of Cu, Pb and Cd in contaminated soil. *Journal of Hazardous Material*, 346: 273-284.
- 60. Miretzky, P. and Fernandez-Cirelli, A. (2008). Phosphates for Pb immobilization in soils: a review. *Environmental Chemistry Letters*, 6(3): 121-133.
- 61. Mohd Idrus, N. F. M., Jamion, N. A., Omar, Q., Sheikh Md Ghazali, S. A. I., Abdul Majid, Z. A. and Yong, S. K. (2018). Magnesium-impregnated biochar for the removal of total phosphorous from artificial human urine. *International Journal of Engineering & Technology*, 7(11): 218-222.